INTEGRATED PLASMA SHAPE AND BOUNDARY FLUX CONTROL ON JET TOKAMAK

MARCO ARIOLA,[a] GIANMARIA DE TOMMASI,[b]* DIDIER MAZON,[c] DIDIER MOREAU,[c]
FABIO PICCOLO,[d] ALFREDO PIRONTI,[b] FILIPPO SARTORI,[d] LUCA ZABEO,[d]
and JET-EFDA CONTRIBUTORS[e]†

[a]*Associazione Euratom-ENEA-CREATE, Università di Napoli Parthenope, via Medina 40, 80133 Napoli, Italy*
[b]*Associazione Euratom-ENEA-CREATE, Università di Napoli "Federico II," via Claudio 21, 80125, Napoli, Italy*
[c]*Euratom-CEA Association, DSM-DRFC, Cadarache, 13108, St. Paul lez Durance, France*
[d]*Euratom-UKAEA Fusion Association, Culham Science Centre, Abingdon OX14 3DB, United Kingdom*
[e]*JET-EFDA, Culham Science Centre, OX14 3DB, Abingdon, United Kingdom*

Advance tokamak scenarios are gaining more and more importance in operating tokamaks. These scenarios pose challenging control problems, since they require the simultaneous achievement of ambitious plasma parameters. The inherent coupling among the various variables calls for an integrated approach for the design of the controllers. This paper describes an example of integrated design recently implemented at JET: the control of plasma shape and boundary flux. After a brief description of the control problem, the paper focuses on the solution that has been adopted, presenting the technical details of the control scheme. The experimental results included in the paper are in agreement with the expected simulation results, and demonstrate the effectiveness of the proposed solution.

KEYWORDS: *tokamak, plasma control systems, plasma boundary flux control*

Note: Some figures in this paper are in color only in the electronic version.

I. INTRODUCTION

Recently, many experiments in operating tokamaks and, as a consequence, a lot of effort in the research on tokamak control, have focused on the so-called advanced tokamak scenarios.[1–3] An advanced tokamak plasma can be defined as a plasma in which the following conditions are simultaneously obtained: a stationary state, a high plasma kinetic pressure, a large fraction of self-driven current, and a sufficiently good particle and energy confinement. Advanced tokamak scenarios are aimed at allowing steady-state operation without the need to drive a large amount of plasma current by external noninductive drive systems, thus making them more efficient.

In the advanced tokamak scenarios, to achieve these simultaneously challenging plasma performance results, several control problems need to be adequately resolved. Among these problems, shape control plays an essential role: First of all, accurate control is needed to obtain the plasma shapes required to achieve high β values[a]; these shapes need to be precisely controlled for a number of reasons, such as optimization of the coupling with the additional heating systems, avoidance of wall interactions, and divertor shape optimization for pumping. This task is complicated by the fact that the "extreme" shapes typically pursued in advanced tokamak scenarios are characterized by a large elongation, which makes even the vertical stabilization difficult to guarantee in the presence of unexpected large disturbances, such as, for instance, edge-localized modes (ELMs). Moreover, to achieve and maintain extreme shapes, the feedback controller needs to regulate many different points all around the plasma boundary.

Another key ingredient to improve the energy confinement and to increase the noninductive current fraction in advanced tokamak regimes is the active control of the internal pressure and current profiles. Since the external current drive sources usually are not sufficient to reach the desired values of noninductive current, the *bootstrap* current[4,5] should be maximized. One way to increase the bootstrap fraction is to generate an internal transport barrier[6,7] (ITB). In the presence of an ITB,

---

[a]β is the ratio of plasma pressure to the magnetic field pressure, and it is one of the figures of merit for magnetic confinement.

there is a reduction of turbulence transport and therefore an increase of confinement. The plasma pressure profile shows a strong internal gradient that produces a bootstrap current peak at the location of the maximum gradient. Some real-time experiments[8] to control the strength of the ITB clearly demonstrated the necessity of controlling at the same time the current density profile. Indeed, the link between ITB triggering and the current density profile is now well known.

In the most sophisticated control schemes presently adopted on tokamaks,[9,10] the current profile control is obtained using feedback controllers that make use of the additional heating devices available on the machine. The inherent, unavoidable coupling among the feedback loops calls for a cautious design of the various controllers; whereas some feedback controllers can be designed neglecting the presence of other loops, more typically the controllers interfere with each other. In these cases, when the controlled and the control variables cannot be tightly separated, the best approach is the integrated design of the various controllers. This approach implies that when a certain feedback loop is tuned, it must take into account all the other loops that can interact with it.

This paper presents an example of integration between two control loops performed at the Joint European Torus (JET): the plasma shape control and the boundary flux control. Most present tokamaks operate inductively with current control; steady-state discharges should in principle be fully noninductive. These discharges call for new operational methods that maintain constant zero loop voltage at the plasma boundary, as has been demonstrated at Tore Supra,[11] DIII-D (Ref. 12), and JT60-U (Ref. 13). Therefore, obtaining effective and routine boundary flux control is an essential step in advanced tokamak regimes. For this reason, at JET an integrated approach for the control of the plasma shape and boundary flux has been developed, implemented, and tested on a high-triangularity ITER-relevant plasma.[14]

The paper is divided as follows. In Sec. II, after a brief introduction on the poloidal field coils system, the JET shape controller (SC) is described,[15] focusing on its structure and its different control modes. Special attention is then given to the new eXtreme Shape Controller (XSC), which is now available at JET and whose architecture has been used to implement the plasma boundary flux control loop. Section III describes the way the boundary flux controller has been designed. Finally, Sec. IV presents the experimental results recently obtained at JET, comparing them with the simulations carried out with XSC Tools[16] during the controller design phase.

II. THE JET TOKAMAK

This section gives an overview of the JET experiment, as well as a description of the plasma shape control system. A full description of the JET tokamak can be

found in Ref. 17, and some experimental results recently achieved on that machine are reported in Refs. 18 and 19. A technical description of JET systems can be found in Ref. 20. More details about plasma current, position, and shape control at JET can be found in Ref. 21, and the XSC algorithm is fully described in Ref. 22.

The JET tokamak was constructed in the late 1970s and early 1980s with the aim of defining the parameters, size, and working conditions of a tokamak reactor. This was to include the study of alpha heating, which implies a reasonable amplification factor Q, which is defined as the ratio of the fusion power to the externally applied heating power. In 1997, 16 MW of fusion power were generated by a heating power of 26 MW, corresponding to $Q \cong 0.6$ (Ref. 23). This result was achieved using a deuterium-tritium plasma. Good results have been obtained using deuterium plasmas as well.

Today, JET continues to make a valuable contribution in preparation for the future high-Q operation of ITER (Ref. 14) through the development of plasma scenarios and by addressing key physics and technical issues.

II.A. The Poloidal Field Coil System

In a tokamak machine, the poloidal field (PF) coils are the actuators available to control the plasma current, position, and shape. Figure 1 shows a poloidal cross section of the JET tokamak with the PF coils shown as squares. These coils are linked together into 10 circuits driven by independent power supplies, named P1, P4, IMB, SHA, PFX, D1, D2, D3, D4, and FRFA.

The P1 circuit enables both the plasma inductive formation and the control of the plasma current. FRFA is used to stabilize the plasma vertical unstable mode by means of a feedback loop, while the other eight circuits are used to shape and move the plasma column within the toroidal chamber.

The current in the FRFA circuit is driven by the vertical stabilization controller.[24] The remaining PF circuits are controlled either by the SC or by the XSC to perform both plasma current and shape control, as described in the next sections.

II.B. The JET Shape Controller

The SC drives the current into the PF circuits, and it was conceived as the solution to the shape control problem for the entire discharge.

During the plasma formation process, the SC controls the currents in PF circuits so that they track a set of preprogrammed waveforms. These waveforms have been empirically shown to give a successful breakdown. Afterward a small plasma column is formed and slowly expands to fill the vessel volume. In this phase, since it is difficult to calculate the plasma shape precisely, the SC controls only the plasma current and the radial position. Depending on the experiment, different aspects of the
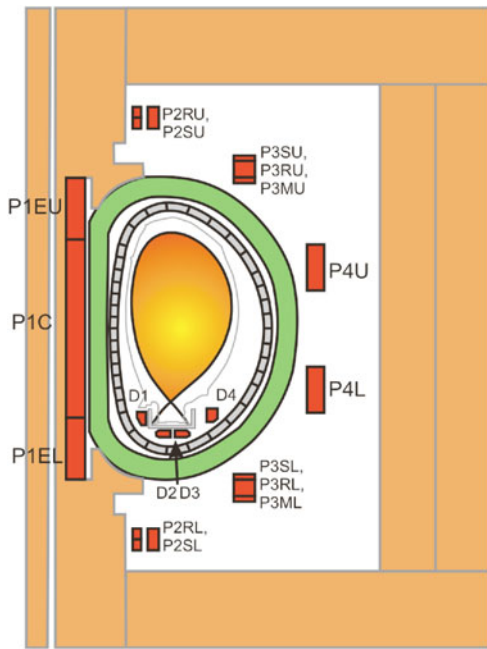
Fig. 1. The JET poloidal field coil system. The P1 circuit includes the elements of the central solenoid, P1EU, P1C, and P1EL, as well as P3MU and P3ML. The series circuit of P4U and P4L is named P4, and the circuit that creates an imbalance current between the two coils is referred to as IMB. SHA is made of the series circuit of P2SU, P3SU, P2SL, and P3SL. The fast radial field circuit, termed FRFA, connects P2RU, P3RU, P2RL, and P3RL. The central part of the central solenoid contains an additional circuit named PFX, which is used for plasma shape control. Finally, the four divertor coils (D1 to D4) are each driven separately by one power supply.
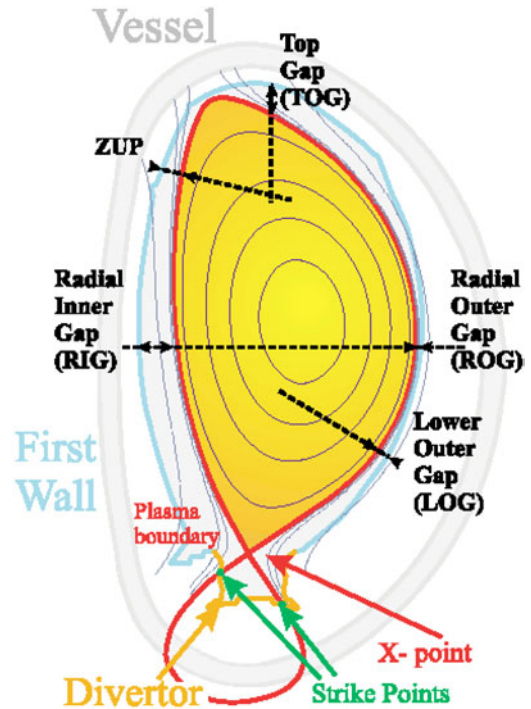

Fig. 2. Plasma shape descriptors at JET. Note that a gap is not strictly the distance between the plasma surface and a point on the wall, but rather the distance measured on a fixed line. This definition simplifies the calculation and provides a good linear relationship between the currents in the PF coils and the geometrical descriptors. Even though the XSC can control up to 32 gaps, for clarity only a few are shown in this figure.

shape become more important. The main experimental phase typically starts after the plasma becomes bounded by a separatrix, and the control is switched to the geometrical descriptors that specify the plasma boundary (gaps, strike points, and *X*-point position shown in Fig. 2).

The SC gives the possibility of controlling simultaneously up to six geometrical descriptors. This limitation has been overcome by the XSC deployed at JET in 2003; as explained later, with this new system it is possible to control, in a mean-square sense, more than 30 plasma shape descriptors using eight PF circuits.

The person responsible for implementing an experiment (the session leader) programs the discharge, dividing it into a number of time windows; in each time window, the PF circuits can be used in one of the following control modes:

1. *Current control*: The controlled variable is the current in the corresponding circuit; this is the case, for instance, of the breakdown phase.

2. *Plasma current control*: The controlled variable is the plasma current.

3. *Gap control*: The controlled variable is a plasma boundary geometrical descriptor, typically a gap.

4. *Blocked*: The current in the actuator is set to 0.

5. *Free-wheeling*: The voltage across the coil is set to 0.

The definition of the variables that can be selected in gap control mode, as well as the availability of the different control modes, differs for each PF circuit. For example, the plasma current control mode is available only for the P1 circuit.

The SC design is based on a plasma linear model; only one model is used for all the cases of interest. The SC designers managed to obtain a controller that guarantees acceptable dynamic performance[25] in many different situations. This result has been achieved while limiting the control bandwidth and tuning the controller parameters during the SC commissioning phase. The session leader is able to obtain the desired plasma configuration

by choosing different control variables in different time windows of the experiment.

The SC design is based on the model of the PF coil system, which can be written as

$$
\mathbf{V}_{PF}(t) = \begin{bmatrix} L_1 & M_{12} & \dots & M_{1N} \\ M_{12} & L_2 & \dots & M_{2N} \\ \vdots & \vdots & \ddots & \vdots \\ M_{1N} & M_{2N} & \dots & L_N \end{bmatrix} \dot{\mathbf{I}}_{PF}(t)
$$

$$
+ \begin{bmatrix} R_1 & 0 & \dots & 0 \\ 0 & R_2 & \dots & 0 \\ \vdots & \vdots & \ddots & \vdots \\ 0 & 0 & \dots & R_N \end{bmatrix} \mathbf{I}_{PF}(t)
$$

$$
= \mathbf{M}\dot{\mathbf{I}}_{PF}(t) + \mathbf{R}\mathbf{I}_{PF}(t) \ , \tag{1}
$$

which is valid in the absence of plasma. The terms L_i represent the self-inductance of the i-th circuit, while M_{ij} is a mutual inductance term. $\mathbf{V}_{PF}(t)$ is the vector of power supply output voltages, $\mathbf{I}_{PF}(t)$ is the vector of measured currents in the PF coils, and R_i are the circuit resistances.

The control algorithm implemented by the SC, which is independent of the choice of control modes, is given by

$$
\mathbf{V}_{ref}(t) = \hat{\mathbf{R}}\mathbf{I}_{PF}(t) + \mathbf{K}(\mathbf{Y}_{ref}(t) - \mathbf{Y}(t)) \ . \tag{2}
$$

In Eq. (2), $\mathbf{V}_{ref}(t)$ are the voltage references to the amplifiers; $\hat{\mathbf{R}}$ is an estimation of matrix $\mathbf{R}$ in Eq. (1); $\mathbf{K}$ is the gain matrix; and $\mathbf{Y}_{ref}(t)$ and $\mathbf{Y}(t)$ are the reference signals and measurements, respectively, and depend on the controlled variable choices. A schematic of the SC is shown in Fig. 3.

The control matrix $\mathbf{K}$ is constructed according to

$$
\mathbf{K} = \hat{\mathbf{M}}\mathbf{T}^{-1}\mathbf{\Lambda} \ , \tag{3}
$$

where $\hat{\mathbf{M}}$ is an estimation of the mutual inductance matrix in Eq. (1) and decouples the PF circuits, $\mathbf{\Lambda}^{-1}$ is the diagonal matrix of desired time constants, and $\mathbf{T}$ is the transformation matrix, which represents the linearized relation between the currents in the PF circuits and the measurements:

$$
\mathbf{Y}(t) = \mathbf{T}\mathbf{I}_{PF}(t) \ . \tag{4}
$$

Replacing Eq. (4) into Eq. (1), the open-loop system model reads

$$
\mathbf{M}\mathbf{T}^{-1}\dot{\mathbf{Y}}(t) = \mathbf{V}_{PF}(t) - \mathbf{R}\mathbf{I}_{PF}(t) \ . \tag{5}
$$

Using Eqs. (2) through (5), the closed-loop system can be written as

$$
\dot{\mathbf{Y}}(t) = \mathbf{\Lambda}(\mathbf{Y}_{ref}(t) - \mathbf{Y}(t)) \ . \tag{6}
$$

The model in Eq. (6) is derived neglecting the delays introduced by the power supplies and by the diagnostics and assuming $\hat{\mathbf{R}} = \mathbf{R}$ and $\hat{\mathbf{M}} = \mathbf{M}$.

It follows that for all the PF circuits set in current control mode, the corresponding $\mathbf{Y}(t)$ entries are the PF currents, and the corresponding block in the matrix $\mathbf{T}$ is the identity matrix.

After the plasma is formed, the plasma current circuit should be added into Eq. (1). The SC adopts a simplified model of the plasma current circuit, in which the plasma resistance is neglected and only the mutual inductance with the P1 circuit is retained. Since the plasma current distribution is a function of the magnetic fields, the mutual induction between P1 and the plasma depends on the currents in the circuits. However, this dependence
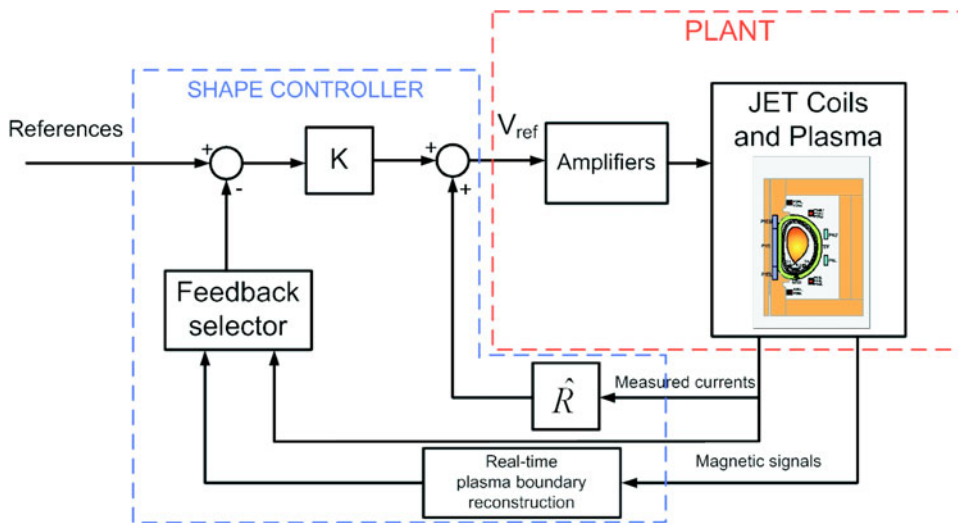

Fig. 3. Block diagram of the JET shape controller. The feedback selector permits to change among the available control modes.

is not relevant, and the following broadly valid linear model can be derived:

$$\dot{I}_p(t) = -c\dot{I}_{\mathrm{P1}}(t) \ , \quad \text{with } c > 0 \ , \qquad (7)$$

where $I_p(t)$ and $I_{\mathrm{P1}}(t)$ are the plasma current and the current in the P1 circuit, respectively. The model of Eq. (7) is oversimplified since it does not take into account any plasma internal profile concise parameters, such as, for instance, beta poloidal β_p and the internal inductance l_i (Ref. 26).

Equation (7) is then used to determine the row corresponding to the plasma current in the **T** matrix, when P1 is set in plasma current control mode.

II.C. The XSC

II.C.1. Control Algorithm

The XSC controls the whole plasma shape, specified as a set of geometrical descriptors (typically 32), calculating the PF coil current references. Its design[22] is based on the following plasma linearized state space model,[27,28] which relates the variations of the PF currents to the variations of the geometrical descriptors around a given equilibrium:

$$\delta\dot{\mathbf{x}}(t) = \mathbf{A}\delta\mathbf{x}(t) + \mathbf{B}\delta\mathbf{u}(t) \qquad (8)$$

and

$$I_{p_{eq}}\delta\mathbf{g}(t) = \mathbf{C}\,\delta\mathbf{I}_{\mathrm{PF}}(t) \ , \qquad (9)$$

where

$$\mathbf{A}, \mathbf{B}, \mathbf{C} = \text{model matrices}$$

$$\delta\mathbf{x}(t) = \left[\delta\mathbf{I}_{\mathrm{PF}}^T(t)\,\delta I_p(t)\right]^T \in \mathbb{R}^{(n_{\mathrm{PF}}+1)}$$

= state space vector, which includes the currents in the n_{PF} (= 8) PF circuits available for the plasma shape control, and the plasma current I_p

$$\delta\mathbf{u}(t) = \left[\delta\mathbf{V}_{\mathrm{PF}}^T(t)\,0\right]^T \in \mathbb{R}^{(n_{\mathrm{PF}}+1)}$$

= input voltages vector

$$\delta\mathbf{g}(t) \in \mathbb{R}^{n_G} = n_G(\leq 32) \text{ shape descriptors variations}$$

$$I_{p_{eq}} = \text{equilibrium value of the plasma current.}$$

The model of Eqs. (8) and (9) is obtained neglecting the effects of the plasma profile parameters $\delta\beta_p(t)$ and $\delta l_i(t)$, which can be regarded as disturbances.

Let $\mathbf{I}_{\mathrm{PF}_N}(t)$ be the PF currents normalized to the equilibrium plasma current; it follows that

$$\delta\mathbf{g}(t) = \mathbf{C}\,\delta\mathbf{I}_{\mathrm{PF}_N}(t) \ . \qquad (10)$$

From Eq. (10) it follows that the plasma boundary descriptors have the same dynamic response as the PF currents.

The shape controller design has been based on the **C** matrix. It is worth noting that the plasma is a non-right-invertible plant, since $n_{\mathrm{PF}} < n_G$; i.e., the number of independent control variables is less than the number of outputs to regulate. For such a plant it is not possible to track a generic set of references with zero steady-state error.

Hence, given a generic set of references, the best performance that can be achieved in steady state is to control to zero the error on n_{PF} linear combinations of geometrical descriptors. Controlling to zero such an error is equivalent to minimizing the following steady-state performance index[29]:

$$J = \lim_{t\to+\infty} (\delta\mathbf{g}_{ref} - \delta\mathbf{g}(t))^T(\delta\mathbf{g}_{ref} - \delta\mathbf{g}(t)) \ , \qquad (11)$$

where $\delta\mathbf{g}_{ref}$ are constant references to the geometrical descriptors.

Minimization of Eq. (11) can be attained using the singular value decomposition (SVD) of the **C** matrix:

$$\mathbf{C} = \mathbf{U}\mathbf{S}\mathbf{V}^T \ ,$$

where the matrix **S** contains the singular values and **U** and **V** are unitary matrices; that is,

$$\mathbf{U}\mathbf{U}^T = \mathbf{U}^T\mathbf{U} = \mathbf{I} \ ,$$

and

$$\mathbf{V}\mathbf{V}^T = \mathbf{V}^T\mathbf{V} = \mathbf{I} \ .$$

As a matter of fact, using the JET linearized models, it turned out that some singular values (typically 2 or 3, depending on the configuration) are one order of magnitude smaller than the others. This fact implies that minimizing the performance index of Eq. (11) retaining all the singular values results in a high control effort at steady state, in terms of PF coil currents. For this reason, the XSC achieves a trade-off condition, minimizing a modified quadratic cost function that penalizes both the error on the controlled shape descriptors and the control effort. This is achieved by controlling to zero the error only for the $\bar{n} < n_{\mathrm{PF}}$ linear combination related to the largest five or six singular values.[29]

A more sophisticated version of the XSC has since been implemented, introducing weight matrices both for the geometrical descriptors and for the PF coil currents. The reason for this lies in the fact that there are some regions of the plasma boundary where more tight requirements are requested, for instance, for the antenna power coupling. Also, the PF coil currents available for feedback purposes differ significantly from coil to coil and among different scenarios. As a consequence, the determination of the controller gains is based on the SVD of the following weighted model output matrix:

$$\tilde{\mathbf{C}} = \tilde{\mathbf{Q}}\mathbf{C}\tilde{\mathbf{R}}^{-1} = \tilde{\mathbf{U}}\tilde{\mathbf{S}}\tilde{\mathbf{V}}^T \ , \qquad (12)$$
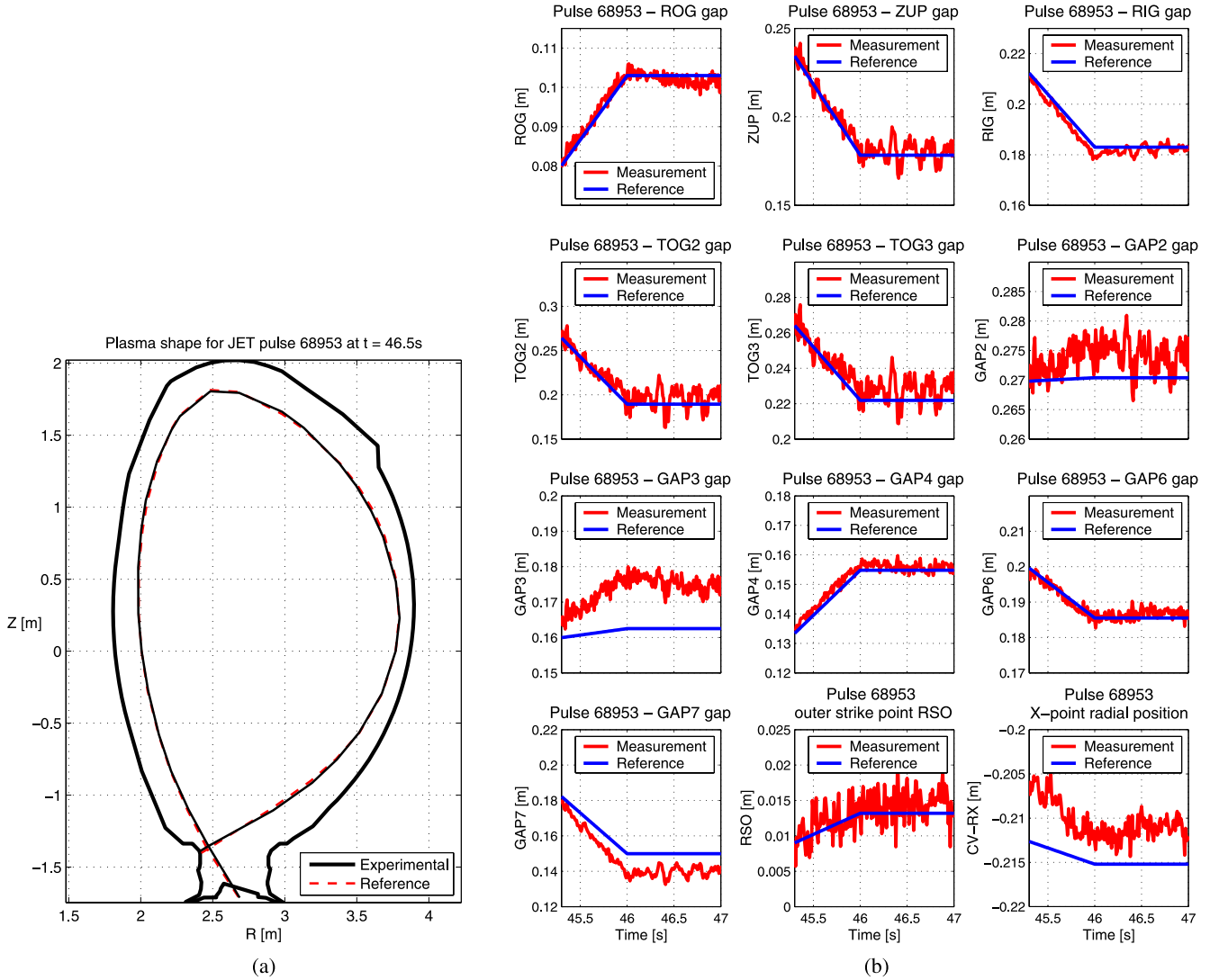
Fig. 4. JET pulse 68953. In this shot the XSC has been used to control the plasma shape. (a) Comparison between the measured shape and the reference at $t = 46.5$ s. (b) Time evolution of 12 plasma shape descriptors. (a) Plasma shape at $t = 46.5$ s and (b) plasma shape descriptor time traces.

where $\tilde{\mathbf{Q}}$ and $\tilde{\mathbf{R}}$ are two diagonal matrices used to weight the errors on the controlled outputs and the currents into the PF coils, respectively. The matrices $\tilde{\mathbf{U}}$, $\tilde{\mathbf{S}}$, and $\tilde{\mathbf{V}}$ are attained by the SVD of the $\tilde{\mathbf{C}}$ matrix.

Hence, the XSC minimizes the cost function

$$\tilde{J}_1 = \lim_{t \to +\infty} (\delta\mathbf{g}_{ref} - \delta\mathbf{g}(t))^T \tilde{\mathbf{Q}}^T \tilde{\mathbf{Q}} (\delta\mathbf{g}_{ref} - \delta\mathbf{g}(t)) \ ,$$

using $\bar{n} < n_{PF}$ degrees of freedom, while the remaining $n_{PF} - \bar{n}$ degrees of freedom are exploited to minimize

$$\tilde{J}_2 = \lim_{t \to +\infty} \delta\mathbf{I}_{PF_N}(t)^T \tilde{\mathbf{R}}^T \tilde{\mathbf{R}} \delta\mathbf{I}_{PF_N}(t) \ .$$

An example of plasma shape controlled by the XSC is reported in Fig. 4, where the experimental results for JET

pulse 68953 are shown. Both the measured shape (solid trace) and the desired reference (dashed trace) are reported in Fig. 4a, and the time traces of 12 plasma geometrical descriptors are shown in Fig. 4b. Note that even if the steady-state error on the whole plasma boundary is not zero, the control error is kept <1 cm for each plasma shape descriptor.

A comparison between the SC and the XSC is reported in Fig. 5. During pulse 67864, the SC was used until $t = 43.5$ s, and the XSC controlled the plasma shape from $t = 43.5$ s, up to the end of the flattop phase.[b] The

---

[b]The flattop phase is such that the plasma current has reached the target value. At the end of the flattop phase, the plasma current starts the rampdown to terminate the pulse.
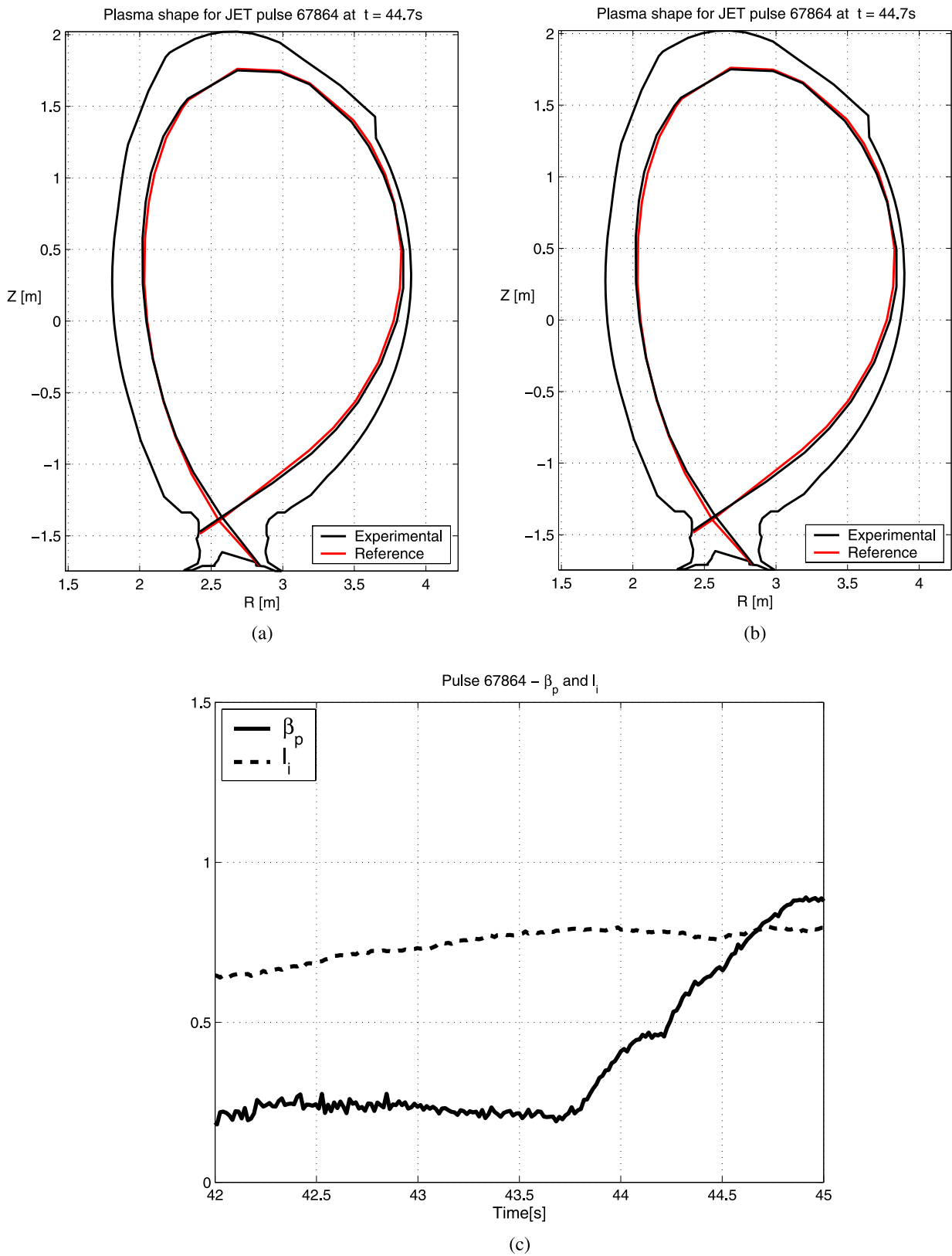
(a)

(b)

(c)

Fig. 5. JET pulse 67864. In this pulse the SC controls the plasma shape until $t = 43.5$ s, and the XSC is used from $t = 43.5$ s up to the end of the flattop phase. (a) Shape at $t = 43.4$ s, when the SC controls the plasma, (b) shape at $t = 44.7$ s, when the XSC controls the plasma, and (c) plasma profile parameters β_p and l_i.
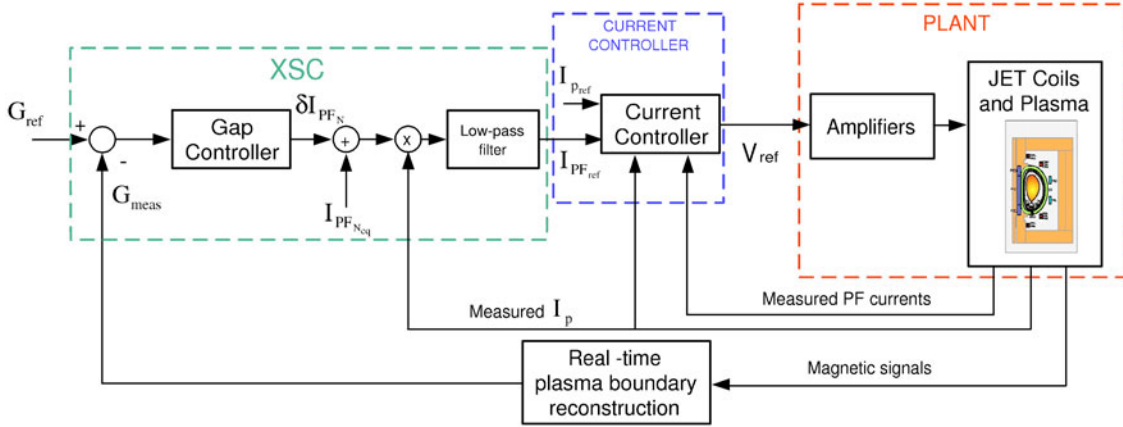
Fig. 6. Block diagram of the XSC.

SC setup adopted during this pulse is the standard one, in which the P1 circuit is set in plasma current control made, four PF circuits are set in gap control mode, and the remaining PF circuits are set in current control mode. Figure 5a shows the measured shape and the desired reference at $t = 43.4$ s, when the SC controls the plasma, Note that in this case, the error between the actual shape and the reference is bigger than that obtained with the XSC, which is shown in Figure 5b. Moreover, note that during the experiment, the disturbances on the shape, which are proportional to time derivatives of the plasma profile parameters β_p and l_i, are bigger when the XSC controls the plasma, rather than when the SC does (see Fig. 5c).

II.C.2. Control Architecture

The XSC has been designed to operate on the JET tokamak; thus, special efforts have been made to minimize the impact on the existing control systems. For this reason the XSC uses the SC to control the currents into the PF coils.

Figure 6 shows the XSC architecture. Here the current controller block is the SC, in which the P1 circuit is set in plasma current control mode and the remaining eight PF circuits are set in current control mode. This block performs both plasma current control and the decoupling of the PF coils circuits; each PF circuit can be treated as an independent SISO (single-input/single-output) channel with a first-order response.

The low-pass filters in Fig. 6 set the time constants for all the PF circuits to the slowest one, τ_{PF}. Therefore, the i-th PF circuit can be modeled as

$$I_{\text{PF}_i}(s) = \frac{1}{1 + s\tau_{\text{PF}}} I_{\text{PF}_{ref_i}}(s) \ ,$$

where $I_{\text{PF}_i}(s)$ and $I_{\text{PF}_{ref_i}}(s)$ are the Laplace transforms of the i-th PF current measurements and reference, respectively.
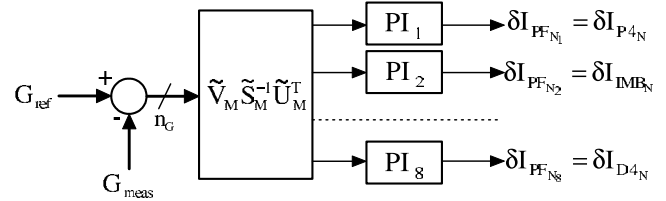

Fig. 7. The XSC gap controller block.

The gap controller block shown in Fig. 6 computes the $\bar{n}$ linear combinations of the geometrical descriptors that are controlled to zero at steady state. These $\bar{n}$ controlled quantities are then projected onto the PF current space.

The structure of the gap controller is depicted in Fig. 7, where the matrices $\widetilde{\mathbf{V}}_M$, $\widetilde{\mathbf{S}}_M$, and $\widetilde{\mathbf{U}}_M^T$ correspond to the $\bar{n}$ largest singular values of the SVD in Eq. (12), and where eight single-input–single-output proportional integral (PI) controllers are used instead of the needed $\bar{n}$. With this architectural choice, it is possible to exploit the antiwindup system of the integral actions to constrain the PF currents between the operational limits.

In particular, the output of the i-th PI is given by

$$\delta I_{\text{PF}_{N_i}}(t) = k_P \tilde{\mathbf{v}}_{M_i}^T \widetilde{\mathbf{S}}_M^{-1} \widetilde{\mathbf{U}}_M^T (\delta \mathbf{g}_{ref}(t) - \delta \mathbf{g}(t))$$

$$+ k_I \int_0^t \tilde{\mathbf{v}}_{M_i}^T \widetilde{\mathbf{S}}_M^{-1} \widetilde{\mathbf{U}}_M^T (\delta \mathbf{g}_{ref}(\sigma) - \delta \mathbf{g}(\sigma)) \, d\sigma \ ,$$

$$(13)$$

where k_P and k_I are the PI gains,[c] and $\tilde{\mathbf{v}}_{M_i}^T$ is the i-th row vector of matrix $\widetilde{\mathbf{V}}_M$.

---

[c] Note that the PIs are the same for all the channels.

The i-th PF current reference to the current controller block is given by

$$I_{\mathrm{PF}_{ref_i}}(t) = I_p(t)(I_{\mathrm{PF}_{N_{eqi}}} + \delta I_{\mathrm{PF}_{N_i}}(t)) \ .$$

The vector of the PF current references $\mathbf{I}_{\mathrm{PF}_{ref}}$ is equal to the vector $\mathbf{Y}_{ref}(t)$ in Eq. (2), which is then used to compute the voltage references to the power amplifiers.

III. BOUNDARY FLUX CONTROL

This section deals with the design of the boundary flux controller for the JET tokamak, and it also describes how this controller has been implemented using the XSC architecture presented in Sec. II.C. This solution enables the simultaneous control of the entire plasma shape and of the magnetic boundary flux.

The actuator that has been chosen to control the plasma boundary flux ψ_b is the current in the P1 circuit. Indeed, an analysis of the influence of the currents on the boundary flux has shown that the other circuits are much less efficient, and therefore it is valuable to use them for the shape control.

As was shown in the previous section, the standard configuration of the XSC makes use of eight PF circuits to control the plasma shape, while the control of the P1 circuit is left to the SC for the plasma current regulation. When controlling ψ_b, the SC releases the control of the P1 current to the XSC, setting this circuit to current control mode. A new actuator is then available to the XSC and it is used to control ψ_b, with negligible influence on the shape. Note that when the XSC controls ψ_b, the plasma current is not feedback controlled, and it is left floating between given bounds.

The first step for the design of the boundary flux controller is the determination of a dynamic model that relates the boundary flux ψ_b to the current in the P1 circuit.

To determine such a model, both ψ_b and I_{P1} are added to the linear model Eqs. (8) and (9). It follows that for the boundary flux control, nine PF coil are used, and the model output equation is given by
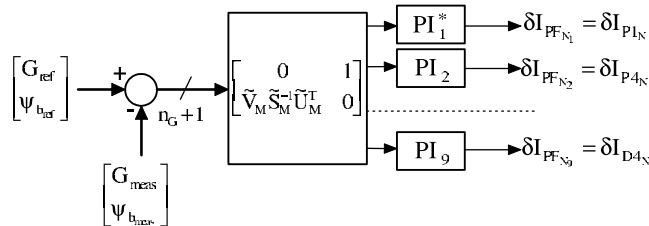
$$\begin{bmatrix} \delta \mathbf{g}(t) \\ \delta \psi_b(t) \end{bmatrix} = \mathbf{C}_{\psi_b} \begin{bmatrix} \delta I_{\mathrm{P1}} \\ \delta \mathbf{I}_{\mathrm{PF}} \end{bmatrix} \ .$$

For the boundary flux controller design, it is necessary to have a SISO model in the form

$$\delta \psi_b(s) = W(s)\delta I_{\mathrm{P1}}(s) \ , \qquad (14)$$

with the transfer function $W(s)$ of order as low as possible, to make the design easier. To arrive at a model in the form Eq. (14), the first step is to consider the loop consisting of the XSC and the plant model (see the scheme in Fig. 6). Then a model order reduction is needed so that a low-order model is obtained. In this case, a balanced model reduction[30] has been performed, arriving to a model of the fourth order.

Basing on the model of Eq. (14), a PI controller has been designed using the root-locus technique.[31] The controller performance have been assessed by means of simulations carried out using the plasma full-order model; these simulations have shown that trying to improve the performance of the boundary flux controller using higher gains in the PI controller induces dangerous oscillations on the PF coil current. For this reason, a compromise solution has been adopted.

The boundary flux controller has been implemented within the XSC architecture shown in Fig. 6. When the ψ_b control is switched on, the I_p control is removed from the current controller block, and all the PF circuits, including P1, are set to current control mode. To compute

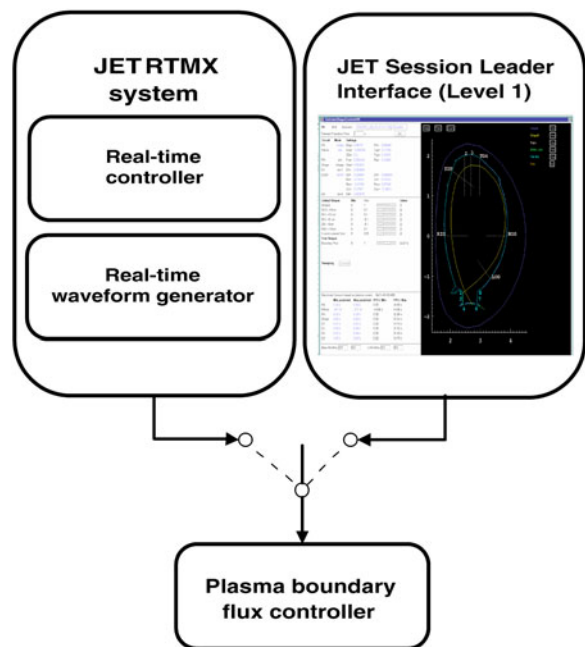Fig. 8. The modified gap controller block for plasma boundary flux control.

Fig. 9. Interconnections between the plasma boundary control system and the JET external systems.
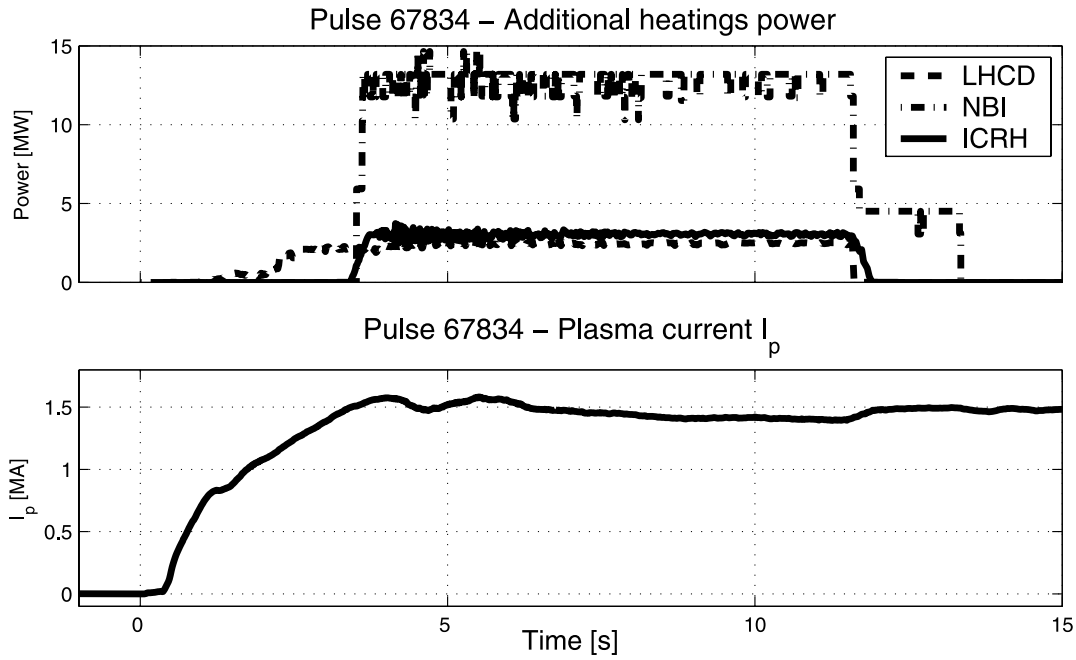
Fig. 10. Additional heating powers and plasma current of JET pulse 67834.

the I_{P1} reference, another channel is added to the gap controller, which is modified as shown in Fig. 8. The gains of the PI controller on the P1 channel (PI_1^*) are different from the ones in Eq. (13), and they are tuned on the model of Eq. (14).

When the XSC is controlling the flux, the plasma current is left floating between safe prescribed bounds; if it exceeds these bounds, a smooth termination of the pulse (soft stop) is triggered.[d]

Eventually, the reference to the plasma boundary flux controller can be generated using one of the two systems shown in Fig. 9:

1. The Real-Time Matlab eXecutor (RTMX) system generates $\psi_{b_{ref}}$ either with a real-time waveform generator or as the output of another real-time control system.

2. The session leader interface allows the generation of ramp references with possibly different slopes in each time window.

IV. EXPERIMENTAL RESULTS

The plasma boundary flux controller was developed at JET in early 2006 and has been used during the 2006

[d]When a soft stop is triggered, the additional heating systems are turned off and the plasma current is brought to zero following a prescribed waveform.
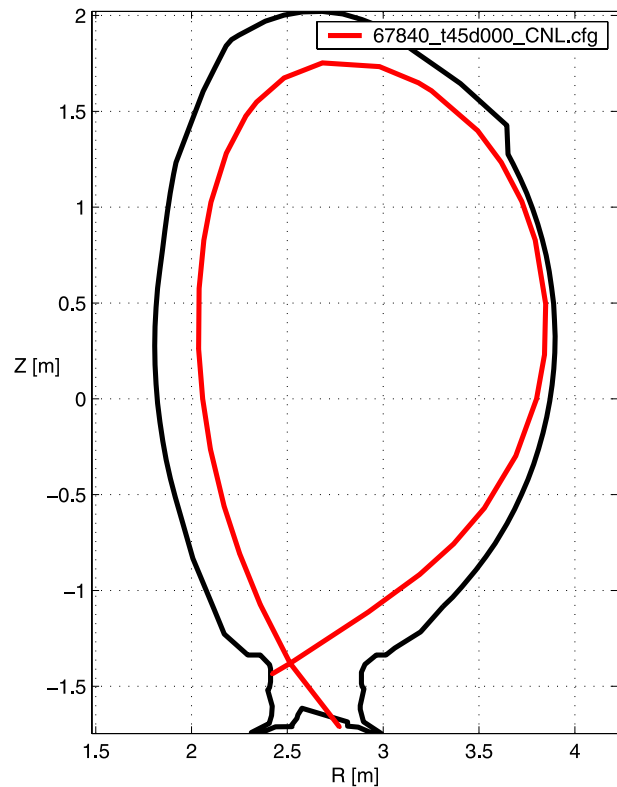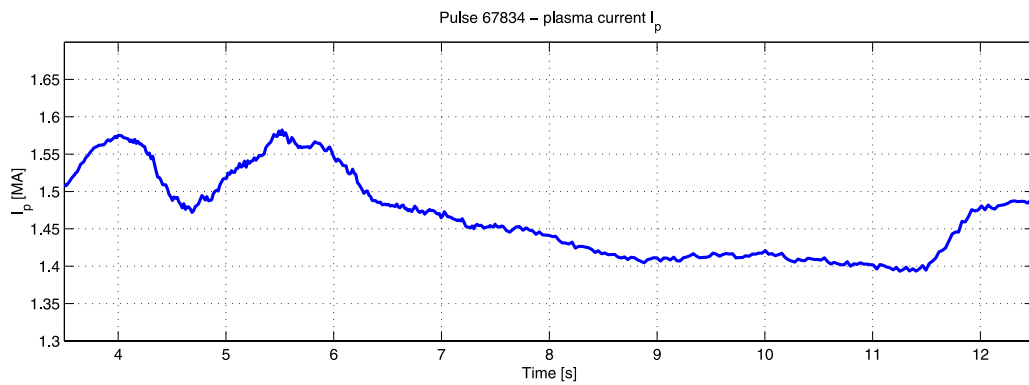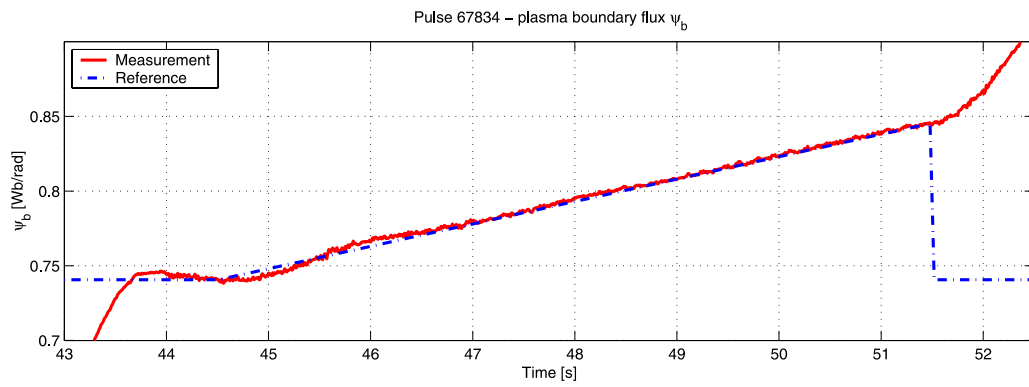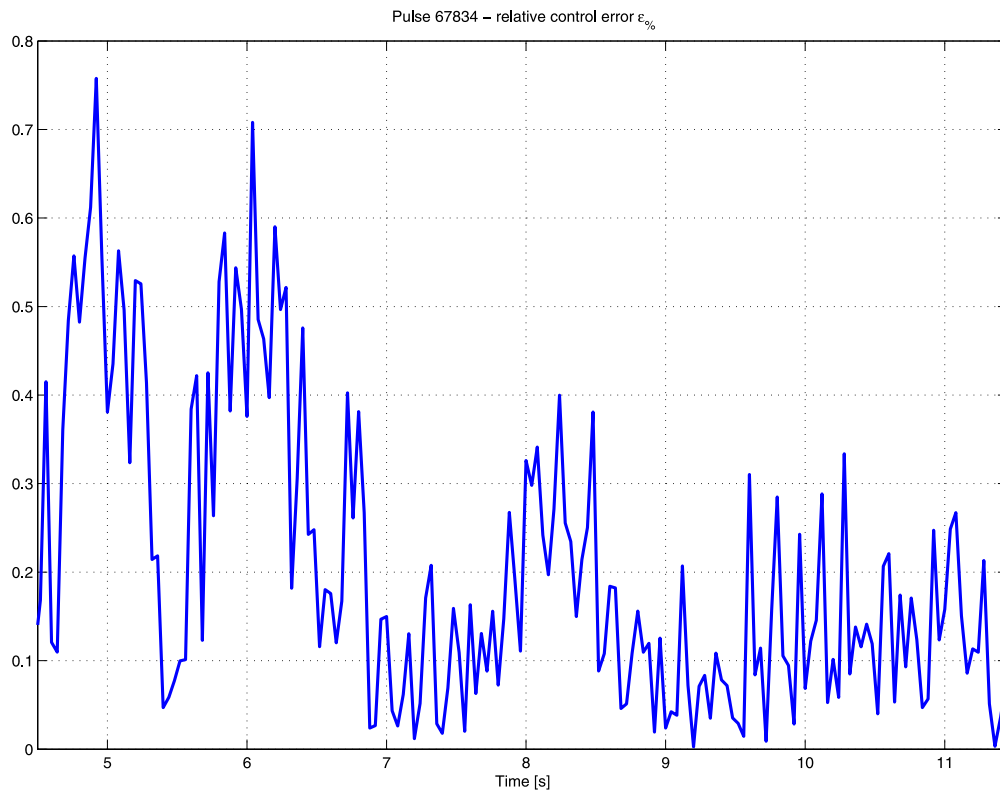

Fig. 11. Plasma shape of JET pulse 67840. This shape has been used for the first boundary flux control experiments at JET.

Fig. 12. JET pulse 67834. Plasma boundary flux control between $t = 44.5$ s and $t = 51.5$ s, with a constant slope ramp reference. (a) Plasma boundary flux $\psi_b(t)$ and current $I_p(t)$ and (b) relative control error $\varepsilon_\%(t)$.

experimental campaigns. Some of the results achieved during these campaigns are presented in this section, together with a comparison between experimental values and simulation results.

The pulses described hereafter were carried out with a toroidal magnetic field $B_T = 3$ T and a nominal plasma current $I_p = 1.5$ MA, while the available additional heating powers during the 10-s plasma current flattop was about 15 MW. The heating power time traces are shown in Fig. 10 for JET pulse 67834. During the preheating phase, which is defined as the time interval between the plasma formation and the main heating phase, only the lower-hybrid current drive (LHCD) actuator is used. Indeed, during the preheating, high-performance plasmas can be obtained with a moderate heating power, achieving the desired target current density profile.[32] At the end of this section is a brief discussion about how the plasma boundary flux control can be effectively used during this phase to improve performance.

The target plasma shape used for the boundary flux control experiments presented in this section is shown in Fig. 11. This shape is a modified version of the one developed for the ITER-relevant scenarios,[33] which allows high plasma density values to be reached, an early formation of a single-null X-point configuration, and the use of non-inductive current drive to tailor the current profile.

The experimental values of both plasma boundary flux $\psi_b(t)$ and current $I_p(t)$ for JET pulse 67834 are shown in Fig. 12a. Here, the reference is chosen as a ramp with a constant slope corresponding to a plasma loop voltage $V_l \cong 95$ mV.

The relative error between the plasma boundary flux reference and measurement,

$$\varepsilon_\%(t) = 100 \left| \frac{\psi_{b_{ref}}(t) - \psi_b(t)}{\psi_{b_{ref}}(t)} \right| ,$$

is shown in Fig. 12b; it becomes smaller than 0.5% after 2 s, which is the settling time of the control system. It is worth noting that the dynamic performance of the boundary flux control is bottlenecked by the bandwidth of the P1 power amplifier.
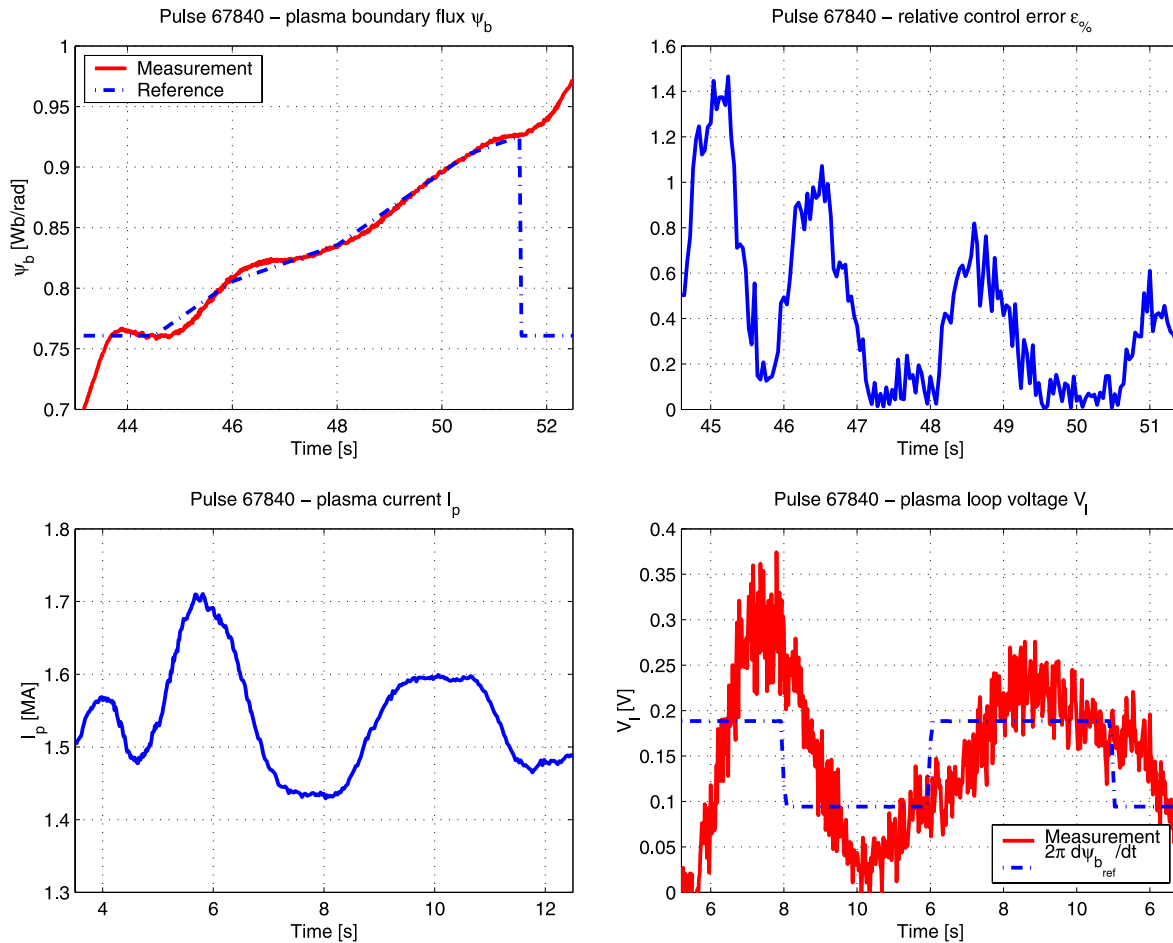

Fig. 13. JET pulse 67840. Boundary flux control is active between $t = 44.5$ s and $t = 51.5$ s, with a variable reference. Note that the desired value for the loop voltage is the time derivative of the plasma boundary flux reference.

Keeping the slope of the boundary flux constant, since the additional heating powers are also constant during the control phase, the plasma current reaches a constant value of $I_p = 1.4$ MA.

The boundary flux control has also been used to perform plasma loop voltage modulations during JET pulse 67840, as shown in Fig. 13. In this case the slope of $\psi_{b_{ref}}(t)$ is varied so as to obtain different values of V_l and I_p. During this experiment the plasma current was left floating between 1.1 and 2.1 MA. Exceeding one of these limits would cause a termination of the pulse.

Although the desired plasma loop voltage $\tilde{V}_l$ is given by the time derivative of the boundary flux reference, i.e., $\tilde{V}_l = d\psi_{b_{ref}}(t)/dt$, the actual controlled variable is $\psi_b(t)$. It follows that the error on the loop voltage is typically higher than the error on the boundary flux.

Figure 14 reports the plasma shape descriptors during the V_l modulation experiment. Although the plasma current acts as a disturbance for the shape control, the error on the shape is kept small.

The results of the plasma loop voltage modulation experiment are in good agreement with the simulation carried out using XSC Tools[16] modified to allow the simulation of both the plasma shape and boundary flux control systems. The simulation results shown in Fig. 15 were obtained using the plasma-linearized model of JET pulse 67834 at $t = 45$ s. In particular, the comparison between the simulated and the experimental values of $\psi_b(t)$ and $I_p(t)$ are shown in Figs. 15a and 15b, respectively. It can be noted that although the simulation of the boundary flux is very accurate, as far as the plasma current is concerned, there is an offset between the simulation and the experiment. This is mainly due to the fact that the estimated plasma resistance used for the simulation is a constant, whereas its actual value changes during the experiment.
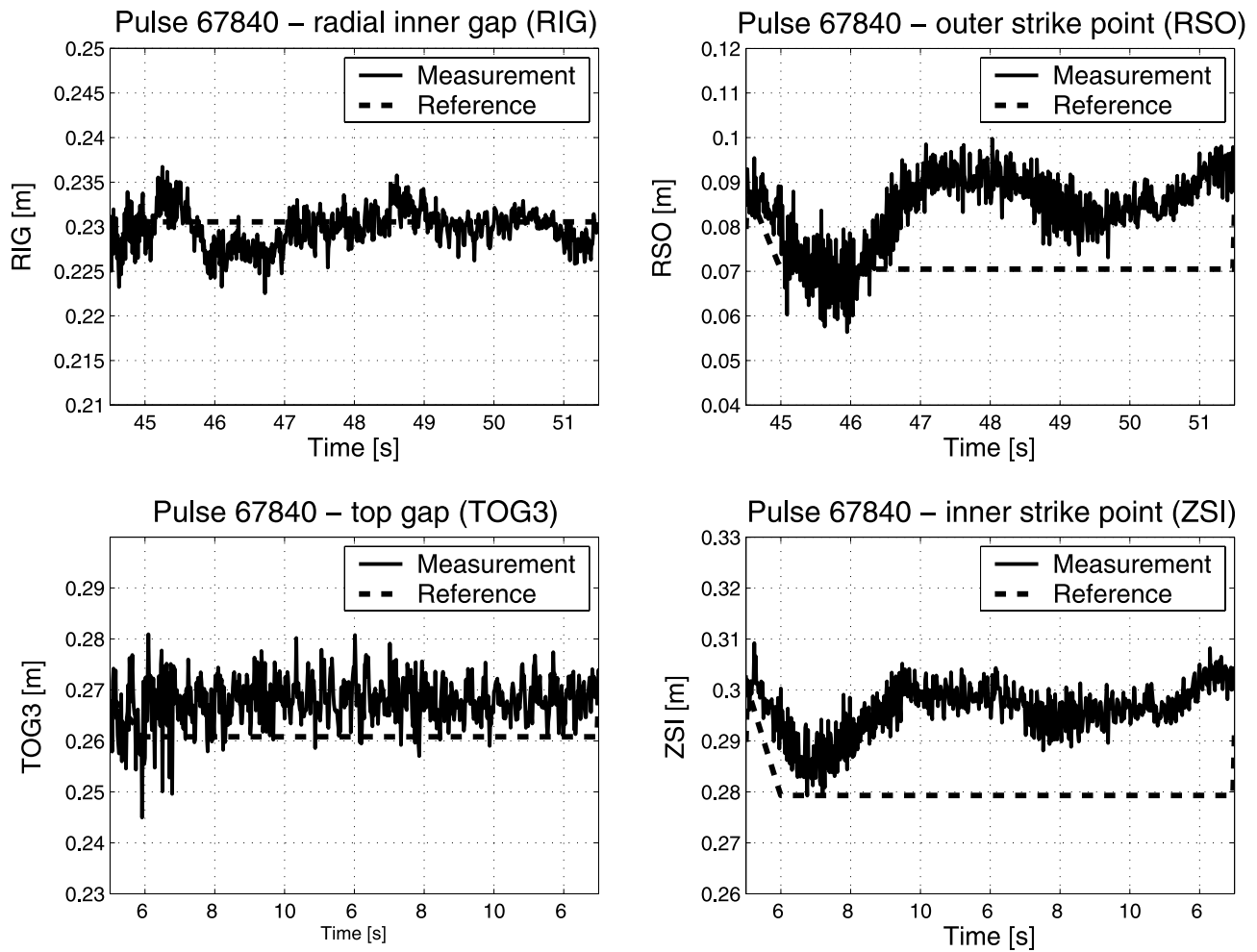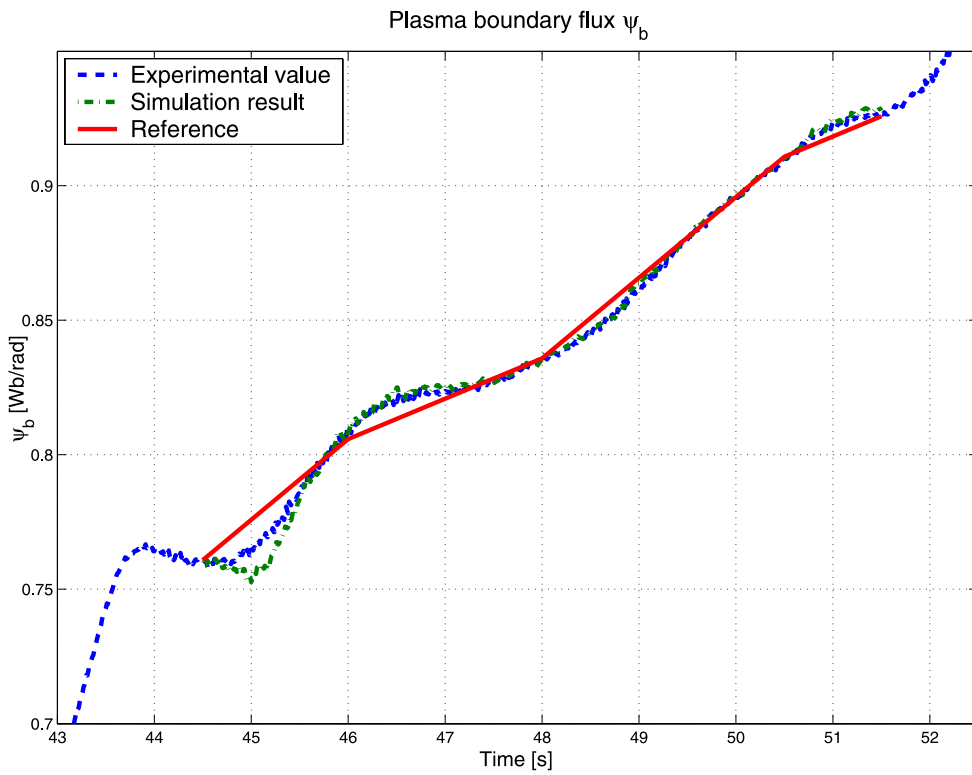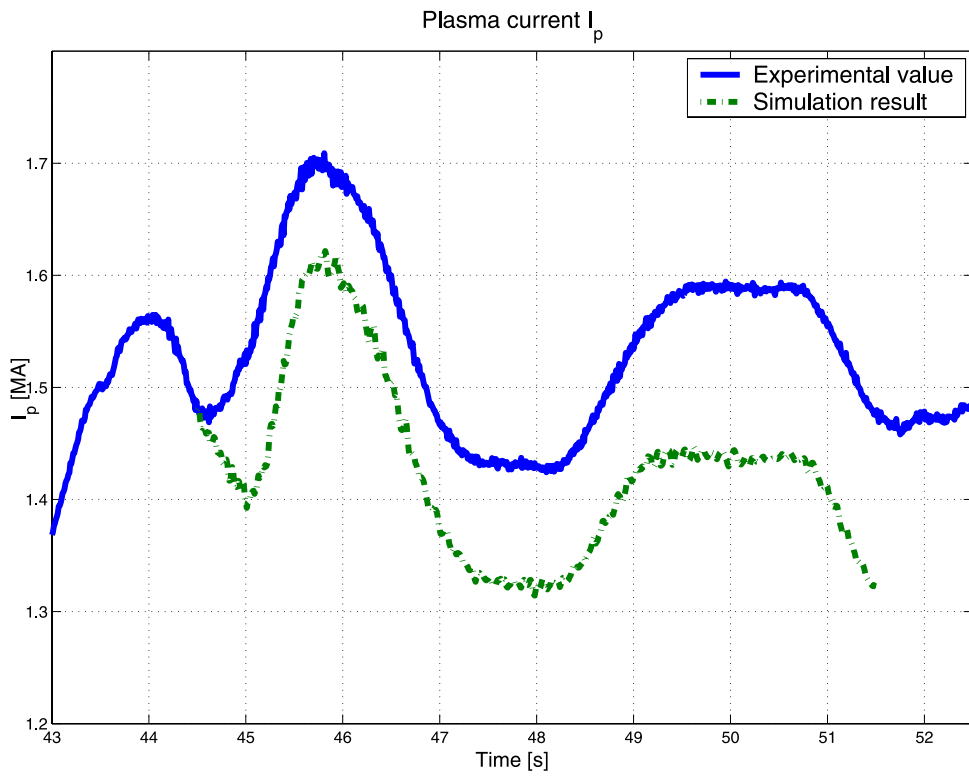

Fig. 14. JET pulse 67840 shape control, showing the behavior of four plasma shape descriptors during the boundary flux control phase.

Fig. 15. Simulation of the plasma loop voltage modulation experiment. The simulation was carried out from $t = 44.5$ s to $t = 51.5$ s using the plasma-linearized model of JET pulse 67834 at $t = 45$ s. (a) Plasma boundary flux $\psi_b(t)$ and (b) plasma current $I_p(t)$.
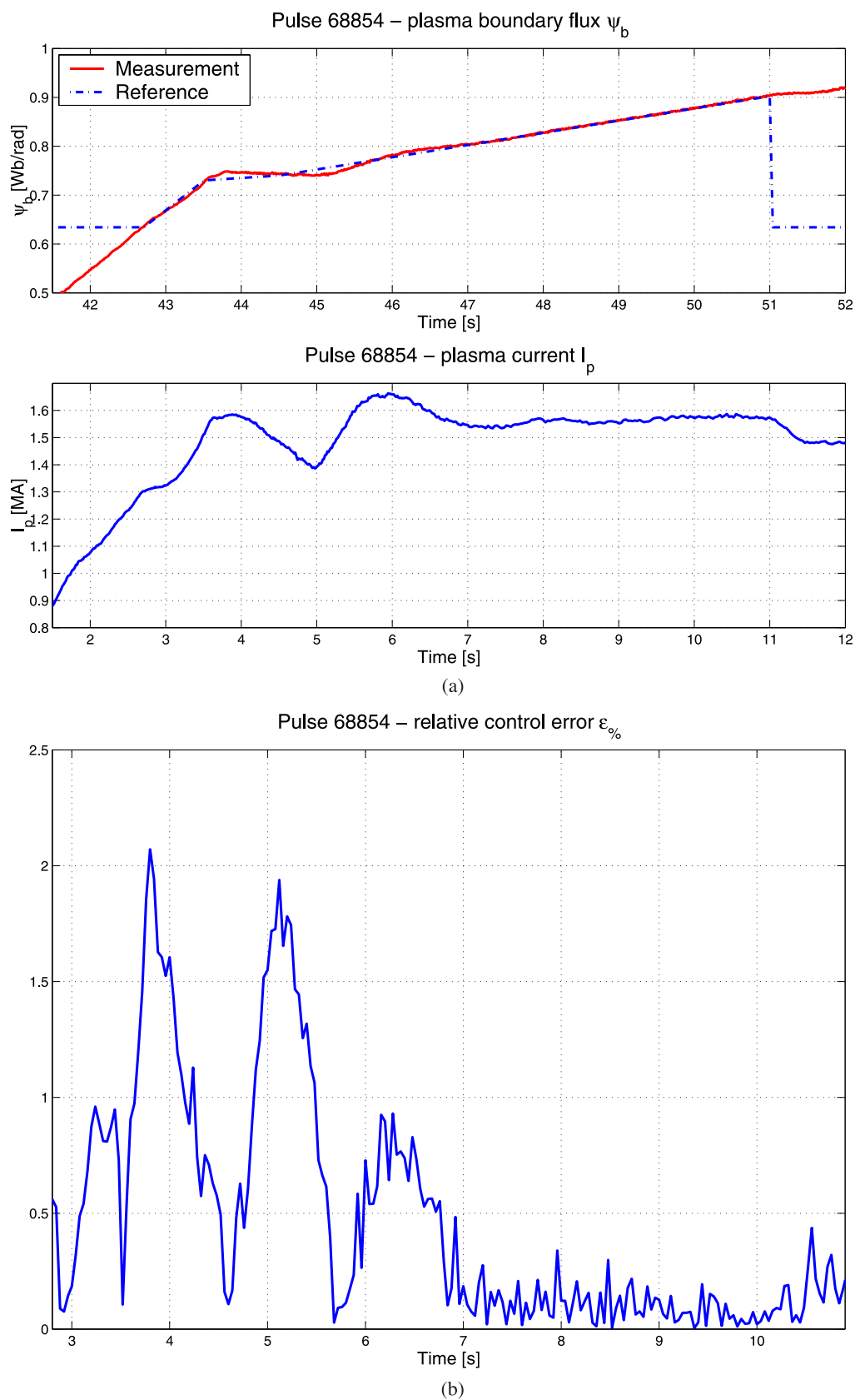
Fig. 16. JET pulse 68854. Boundary flux control starts at $t = 42.7$ s during the plasma current ramp-up phase and stops at $t = 51$ s. (a) Plasma boundary flux $\psi_b(t)$ and current $I_p(t)$ and (b) relative control error $\varepsilon_{\%}(t)$.

During JET pulses 67834 and 67840, the boundary flux control starts during the plasma current flattop phase. In JET pulse 68854 (see Fig. 16), the boundary flux control has been switched on during the plasma current ramp-up phase, and the reference is such that $I_p = 1.6$ MA is obtained.

The ramp-up phase corresponds to the preheating phase; thus, it is very important because it preforms the target current density profile, which is crucial for improving the plasma performance. Future works at JET will be devoted to the integration of plasma shape (including boundary flux) with plasma current profile control.[34] Indeed, controlling the boundary flux ψ_b enables us to control indirectly the plasma current I_p via the edge value of the current density profile. The combination of distributed plasma current density profile and I_p control gives more flexibility in the quest for performance and steady-state discharges.

V. CONCLUSIONS AND FUTURE WORKS

In this paper we have presented an integrated approach for the simultaneous control of plasma shape and boundary flux, recently implemented at JET. This control scheme has been successfully tested during several experiments on high-triangularity ITER-relevant plasmas; different references on the boundary flux have been chosen, either with constant slope or slowly time varying. This integrated control has been tested both during the plasma current flattop phase and during the ramp-up phase.

At JET, in the near future, this controller will be integrated in a more general scheme with the objective of obtaining a centralized controller for the plasma shape, boundary flux, current, and pressure profiles.

REFERENCES

1. T. S. TAYLOR, *Plasma Phys. Control. Fusion*, **39**, B47 (1997).

2. C. GORMEZANO, *Plasma Phys. Control. Fusion*, **41**, B367 (1999).

3. X. LITAUDON, *Plasma Phys. Control. Fusion*, **47**, A1 (2006).

4. R. J. BICKERTON et al., *Nature Phys. Sci.*, **229**, 110 (1971).

5. A. A. GALEEV and R. Z. SAGDEV, *Sov. Phys. JETP*, **26**, 233 (1968).

6. J. W. CONNOR et al., *Nucl. Fusion*, **44**, R1 (2004).

7. R. C. WOLF, *Plasma Phys. Control. Fusion*, **45**, R1 (2003).

8. D. MAZON et al., *Plasma Phys. Control. Fusion*, **44**, 1087 (2002).

9. D. MOREAU et al., *Proc. 20th IAEA Fusion Energy Conf.*, Vilamoura, Portugal (2004).

10. L. LABORDE et al., *Plasma Phys. Control. Fusion*, **47**, 155 (2005).

11. T. WIJNANDS et al., *Nucl. Fusion*, **37**, 777 (1997).

12. C. C. PETTY et al., *Nucl. Fusion*, **35**, 773 (1995).

13. H. TAKENAGA and the JT-60 TEAM, *Proc. 21st IAEA Fusion Energy Conf.*, Chengdu, China (2006).

14. M. SHIMADA et al., *Nucl. Fusion*, **44**, 350 (2004).

15. M. GARIBBA et al., *Proc. 15th SOFE Conf.*, pp. 33–36 (1996).

16. G. DE TOMMASI et al., *IEEE Trans. Plasma Sci.*, **35**, 709 (2007).

17. J. WESSON, *The Science of JET*, JET Joint Undertaking, Abingdon, Oxon, JET-R(99)13 (2000).

18. J. PAMELA, E. R. SOLANO, and JET EFDA CONTRIBUTORS, *Nucl. Fusion*, **43**, 1540 (2003).

19. M. L. WATKINS on behalf of JET-EFDA CONTRIBUTORS, *Proc. 21st IAEA Fusion Energy Conf.*, Chengdu, China (2006).

20. *Fusion Technol.*, **11** (1987), special issue.

21. F. SARTORI et al., *IEEE Control Syst. Mag.*, **26**, 64 (2006).

22. M. ARIOLA and A. PIRONTI, *IEEE Control Syst. Mag.*, **25**, 65 (2005).

23. M. KAILHACKER et al., *Nucl. Fusion*, **39**, 209 (1999).

24. M. LENNHOLM et al., *Proc. 17th SOFE Conf.*, Vol. 1, pp. 539–542 (1997).

25. M. GARIBBA et al., *Fusion Technol.*, **1**, 747 (1994).

26. G. AMBROSINO and R. ALBANESE, *IEEE Control Syst. Mag.*, **26**, 76 (2005).

27. R. ALBANESE and F. VILLONE, *Nucl. Fusion*, **38**, 723 (1998).

28. R. ALBANESE et al., *Fusion Eng. Des.*, **66–68**, 715 (2003).

29. G. AMBROSINO et al., *IET Control Theory Applic.*, **1**, 604 (2007).

30. K. ZHOU and J. C. DOYLE, *Essentials of Robust Control*, Prentice-Hall, Englewood Cliffs, New Jersey (1998).

31. G. FRANKLIN et al., *Feedback Control of Dynamic Systems*, 5th ed., Prentice-Hall, Englewood Cliffs, New Jersey (2006).

32. T. TALA et al., *Plasma Phys. Control. Fusion*, **44**, 1181 (2002).

33. F. G. RIMINI et al., *Nucl. Fusion*, **45**, 1481 (2005).

34. D. MOREAU et al., *Proc. 21st IAEA Fusion Energy Conf.*, Chengdu, China (2006).